Treatment-Dependent Surface Chemistry and Gas Sensing Behavior of the Thinnest Member of Titanium Carbide MXenes

Qian Sun,[a] Jian Wang,[a] Xiang Wang,[a] Jie Dai,[a] Xiaoshan Wang,[a,b] Huachen Fan,[a] Zhiwei Wang,[a,b] Hai Li, *,[a] Xiao Huang*,[a] and Wei Huang*,[a,b]

[a] Key Laboratory of Flexible Electronics (KLOFE) & Institute of Advanced Materials (IAM), Jiangsu National Synergistic Innovation Center for Advanced Materials (SICAM), Nanjing Tech University (NanjingTech), 30 South Puzhu Road, Nanjing 211816, China E-mail: iamxhuang@njtech.edu.cn, iamhli@njtech.edu.cn

[b] Frontiers Science Center for Flexible Electronics, Xi'an Institute of Flexible Electronics (IFE) and Xi'an Institute of Biomedical Materials & Engineering, Northwestern Polytechnical University, 127 West Youyi Road, Xi'an 710072, China. E-mail: iamwhuang@nwpu.edu.cn

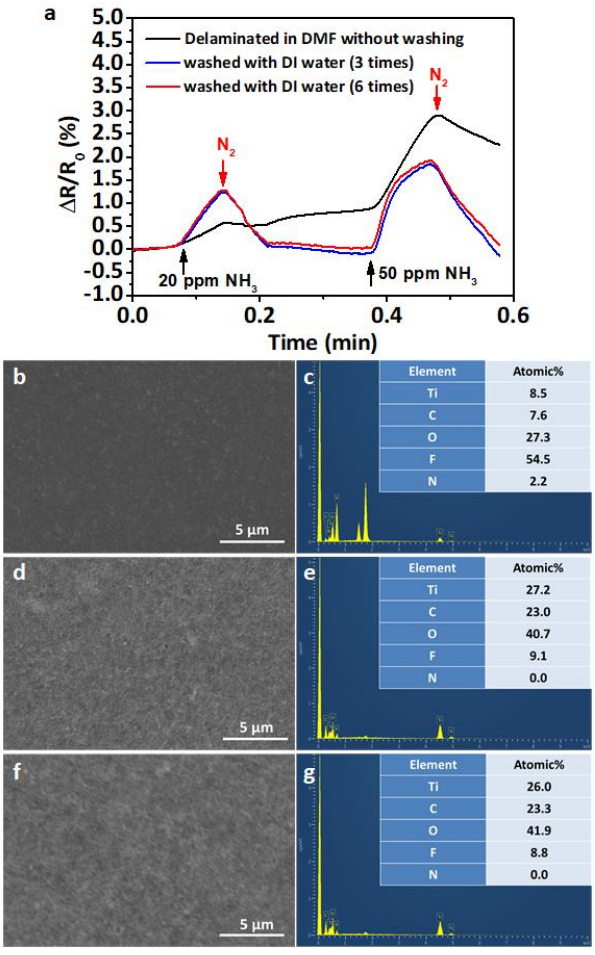

Figure S1. (a) Dynamic response curves of sensors fabricated from Ti_2CT_x (HF) nanosheets without washing, and washed with DI water for 3 and 6 times, respectively, after delaminated in DMF. SEM images (b, d and f) and EDX analyses (c, e and g) of the nanosheets (b and c) without washing, (d and e) washed for 3 times, and (f and g) washed for 6 times.

To study the effect of DMF residual, we tested the sensing performance of Ti_2CT_x (HF) nanosheets exfoliated in DMF without washing, washed for 3 times with water, and washed for 6 times with water, respectively (Figure S1a). The sensor fabricated from Ti_2CT_x (HF) nanosheets without washing showed lower response and poorer desorption as compared with those washed with water. This may be due to the preferred binding of target gas molecules to DMF molecules via inter-molecular interactions. However, there is not much difference in the sensing performance between nanosheets washed for 3 and 6 times; and their corresponding EDS spectra also show no detectable N element (Figure S1b-S1g), indicating the removal of most DMF after washing. Therefore, although DMF had an adverse effect on gas desorption, this effect can be eliminated by washing the nanosheets in water for at least 3 times.

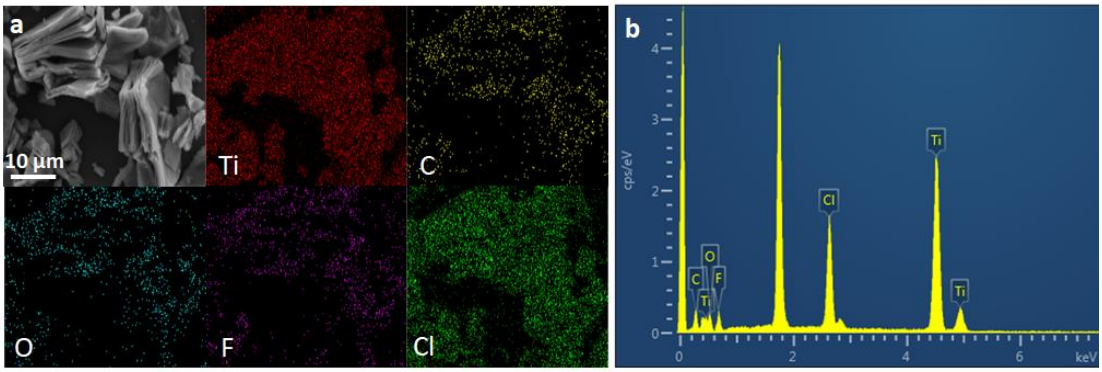

Figure S2. (a) SEM image, EDX mapping and (b) EDX spectrum of typical multi-layered Ti_2CT_x (LiF/HCl) particles, showing the uniform distribution of O, F and Cl elements, while Al has been removed.

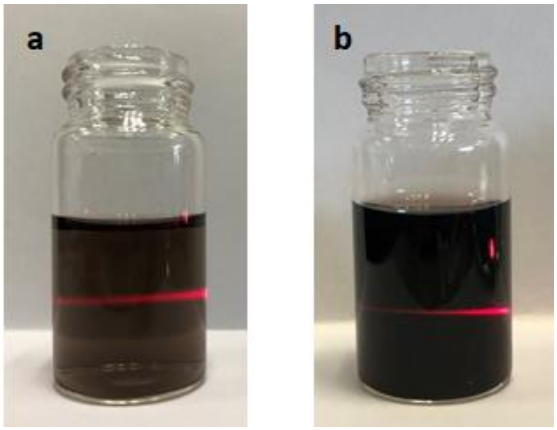

Figure S3. The Tyndall scattering effect shown in colloidal solutions of (a) Ti_2CT_x (LiF/HCl) nanosheets and (b) Ti_2CT_x (HF) nanosheets, suggesting the homogeneity of the dispersions.

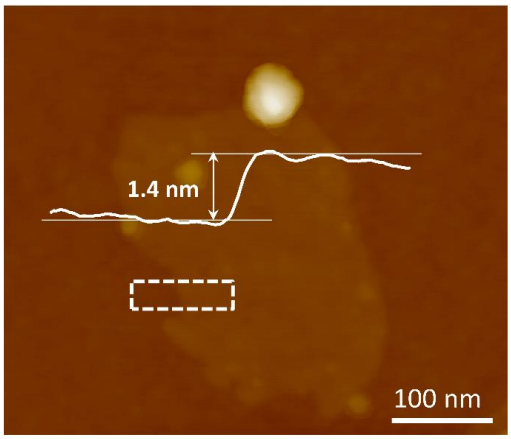

Figure S4. AFM image and height analysis of a typical Ti_2CT_x (LiF/HCl) nanosheet (rectangular region).

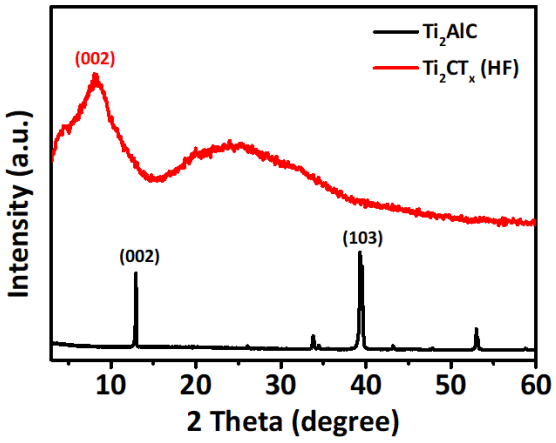

Figure S5. XRD patterns of Ti_2AlC powder and Ti_2CT_x (HF) nanosheets.

Similar to Ti_2CT_x (LiF/HCl), the (002) peak of Ti_2CT_x (HF) as compared to that of Ti_2AlC was shifted to a smaller angle (from 12.9° to 8.3°), suggesting the expansion of the inter-layer spacing (from 6.9 nm to 10.7 nm). This enlarged interlayer spacing corresponds to the thickness of single-layer Ti_2CT_x nanosheets, and also the distance between adjacent layers in few-layer nanosheets bound by the weak van der Waals force. As compared to the Ti_2AlC crystals before Al removal, the exfoliated Ti_2CT_x nanosheets provide larger surface areas for gas adsorption. Besides, the van der Waals larger gap in Ti_2CT_x as compared to the covalent/metallic-bound Ti-Al-Ti interlayer may facilitate the insertion of target gas molecules between layers.[1, 2]

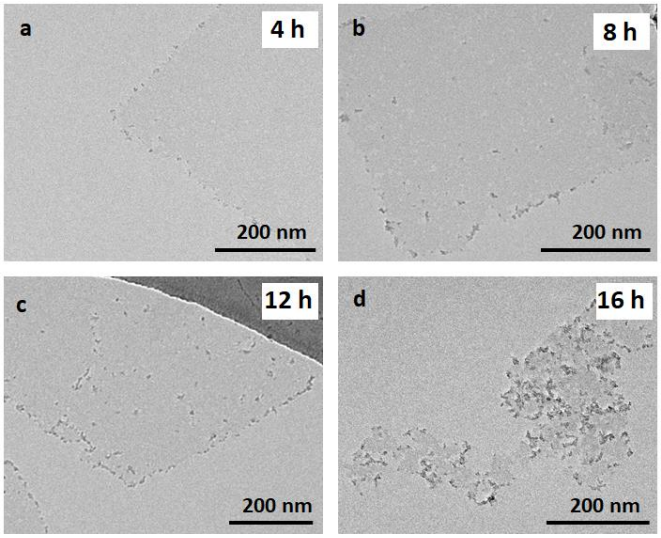

Figure S6. TEM images of TiO_2/Ti_2CTx (LiF/HCl) composites prepared at different reaction time: (a) 4 h, (b) 8 h, (c) 12 h, and (d) 16 h.

The control experiments were carried out to systematically study the oxidation process by characterizing the composite samples obtained at different reaction intervals (Figure S6). It can be seen that the size of the TiO_2 particles did not increase much by prolonging the reaction time, but their loading density increased obviously. The particles started to appear on the edges of the MXene nanosheet at about 4 h, and slowly began to form on the basal plane of the nanosheet. At about 16 h, pores were observed in the nanosheets, and the sheet structure collapsed. The product obtained from 12 h of oxidization possessed a higher loading of TiO_2 and retained the sheet structure. Therefore, this sample was selected for further characterization.

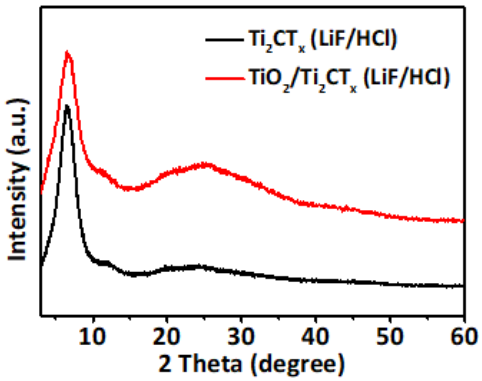

Figure S7. XRD patterns of Ti_2CT_x (LiF/HCl) nanosheets and TiO_2/Ti_2CT_x (LiF/HCl) composites. Note that peaks of TiO_2 are not shown in the pattern of TiO_2/Ti_2CT_x (LiF/HCl), probably due to the small size and poor crystallinity of the TiO_2 nanoparticles.

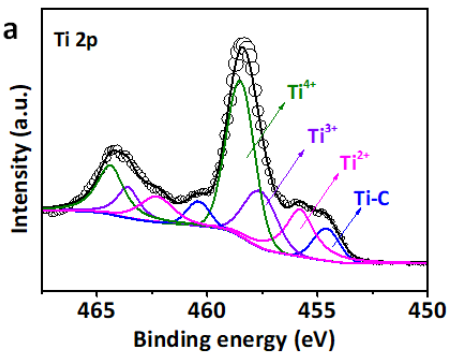

b

Component	Ratio (%)
Ti-C	10.29
Ti^{2+}	22.62
Ti^{3+}	20.84
Ti^{4+} (TiO_2)	46.24

Figure S8. (a) XPS high-resolution Ti 2p spectrum of TiO_2/Ti_2CT_x (LiF/HCl) composites. (b) Table of the concentration of the Ti-based species in TiO_2/Ti_2CT_x (LiF/HCl) composites.

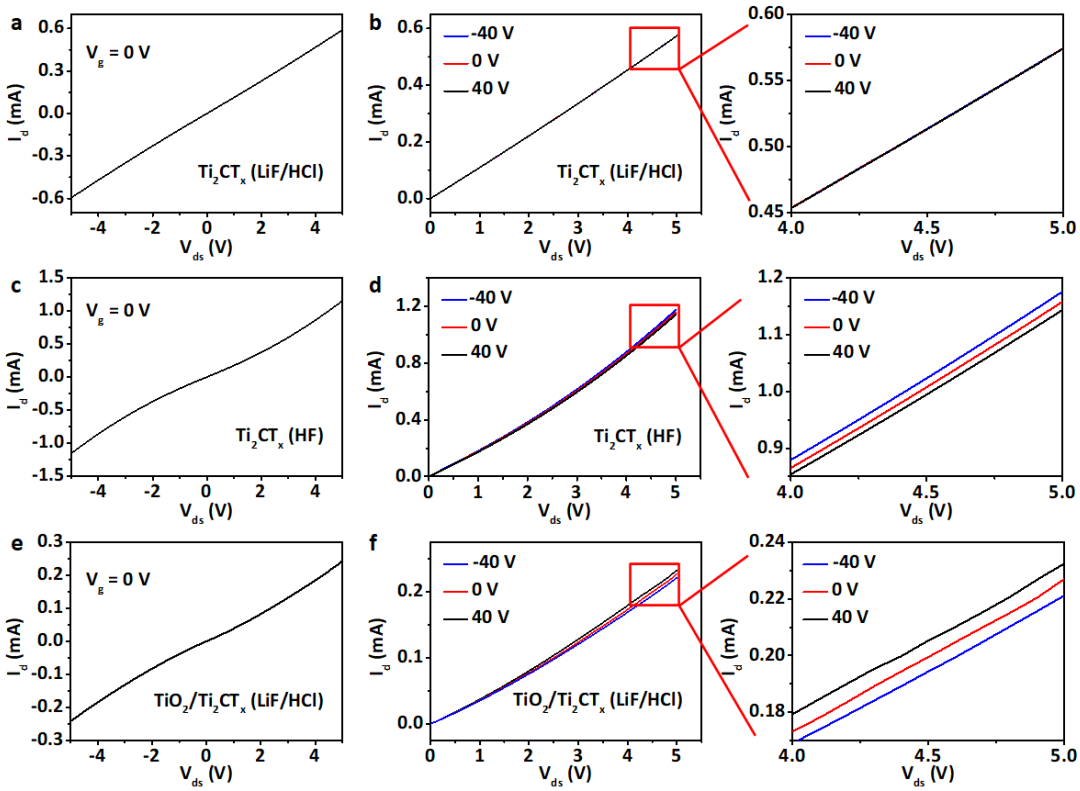

Figure S9. Drain current (I_d) characteristics of back-gated thin film FETs based on (a) Ti_2CT_x (LiF/HCl) nanosheets, (c) Ti_2CT_x (HF) nanosheets and (e) TiO_2/Ti_2CT_x (LiF/HCl) nanosheets for drain-source voltages (V_{ds}) varied from -5 to 5 V at a gate voltage (V_g) of 0 V. The I_d-V_{ds} curves of (b) Ti_2CT_x (LiF/HCl) nanosheets (d) Ti_2CT_x (HF) nanosheets and (f) TiO_2/Ti_2CT_x (LiF/HCl) nanosheets at various V_g ranging from -40 to 40 V, measured under vacuum (5×10^{-5} Torr) at 77 K.

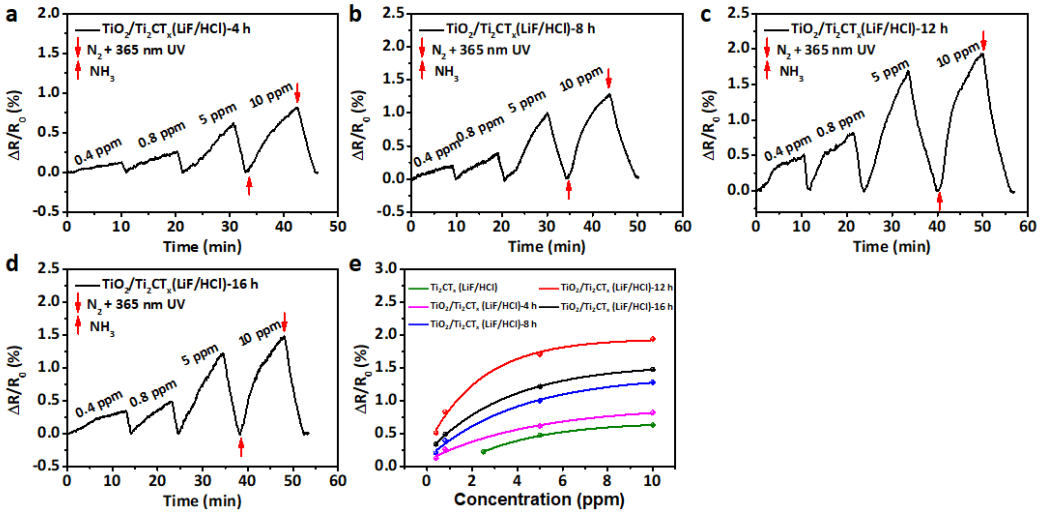

Figure S10. Dynamic response-recovery curves of sensors fabricated from TiO_2/Ti_2CT_x (LiF/HCl) composites prepared at different oxidization time: (a) 4 h, (b) 8 h, (c) 12 h, and (d) 16 h. (e) Normalized change of resistance of different sensors at various NH_3 concentrations.

TiO_2/Ti_2CT_x (LiF/HCl) composites with different TiO_2 loading were achieved by varying the oxidation time (Figure S6). Their corresponding sensing performance is shown in Figure S10. The sensing response toward NH_3 increases as the reaction time increased from 0 to 12 h, and then decreases for the product obtained after 16 h of oxidation. This suggests that too much loading of TiO_2 and loss of the structural integrity of the nanosheets can lead to a reduced sensing performance.

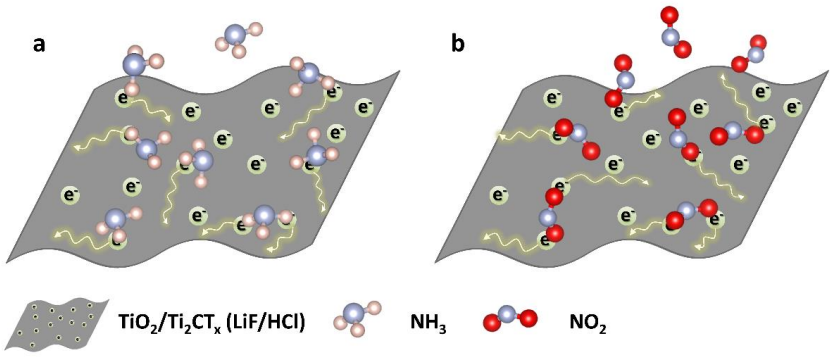

Figure S11. Schematic illustration of the surface charge scattering dominated gas sensing mechanism of TiO_2/Ti_2CT_x (LiF/HCl) toward (a) NH_3 and (b) NO_2.

Table S1. Baseline resistance (R_0) of chemiresistive sensors fabricated from Ti_2CT_x (LiF/HCl), and TiO_2/Ti_2CT_x (LiF/HCl).

Sample	R_0 (Ω)
Ti_2CT_x (LiF/HCl)	~10^3
TiO_2/Ti_2CT_x (LiF/HCl)	~10^5

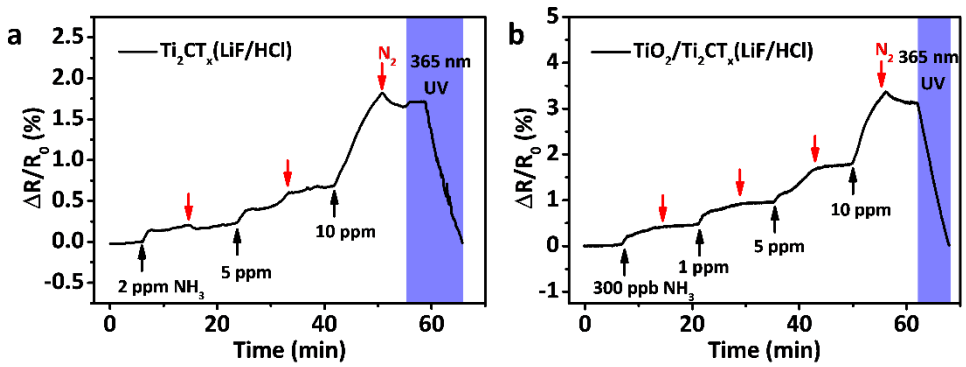

Figure S12. Dynamic response curves of (a) Ti_2CT_x (LiF/HCl) nanosheets and (b) TiO_2/Ti_2CT_x (LiF/HCl) nanosheets fabricated sensors in response to NH_3 with different concentrations, and the UV light-assisted resistance recovery.

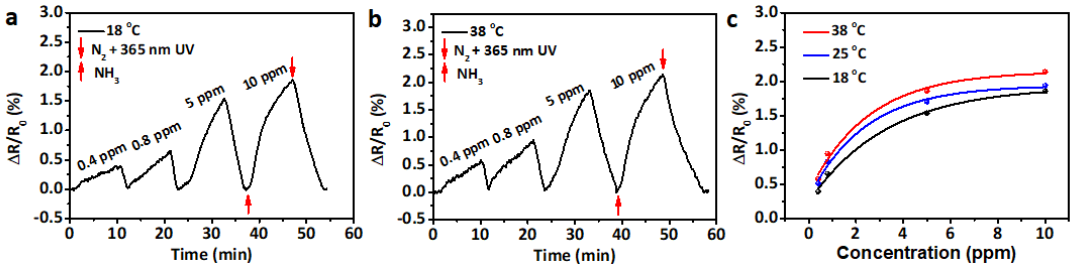

Figure S13. Dynamic response transient of the gas sensor based on TiO_2/Ti_2CT_x (LiF/HCl) to different concentrations of NH_3 at (a) 18 °C and (b) 38 °C. (c) Responses versus NH_3 concentration for TiO_2/Ti_2CT_x (LiF/HCl) based gas sensors at different temperature. It can be seen that by increasing temperature from 18 to 38 °C, an average of ~0.3% increase in the sensing response was observed.

Reference

1. Z. Sun, D. Music, R. Ahuja, S. Li and J. M. Schneider, *Phys. Rev. B*, 2004, **70**, 092102.
2. H. J. Koh, S. J. Kim, K. Maleski, S. Y. Cho, Y. J. Kim, C. W. Ahn, Y. Gogotsi and H. T. Jung, *ACS Sens.*, 2019, **4**, 1365-1372.